High-Precision Measurements of [superscript 33]S and [superscript 34]S Fractionation during SO[subscript 2] Oxidation Reveal Causes of Seasonality in SO[subscript 2] and Sulfate Isotopic Composition

High-precision measurements of ^{33}S and ^{34}S fractionation during SO_2 oxidation reveal causes of seasonality in SO_2 and sulfate isotopic composition

Eliza Harris,[*,†,¶] Bärbel Sinha,[¶,§] Peter Hoppe,[¶] and Shuhei Ono[†]

Department of Earth, Atmospheric and Planetary Sciences, Massachusetts Institute of Technology, 77 Massachusetts Ave, 02139 Cambridge, USA, Laboratory for Air Pollution and Environmental Technology, Swiss Federal Laboratories for Materials Science and Technology, Überlandstrasse 129, CH-8600 Dübendorf, Switzerland, Department of Particle Chemistry, Max Planck Institute for Chemistry, Hahn-Meitner-Weg 1, DE-55128 Mainz, Germany, and Department of Earth Sciences, IISER Mohali, Sector 81, SAS Nagar, Manauli PO 140306, India

E-mail: elizah@mit.edu

Abstract

This study presents high-precision isotope ratio-mass spectrometric measurements of isotopic fractionation during oxidation of SO_2 by OH radicals in the gas phase and H_2O_2 and transition metal ion catalysis (TMI-catalysis) in the aqueous phase. Although temperature dependence of fractionation factors was found to be significant for H_2O_2 and TMI-catalysed pathways, results from a simple 1D model revealed that changing partitioning between oxidation pathways was the dominant cause of seasonality in the isotopic composition of sulfate relative to SO_2. Comparison of modelled seasonality with observations shows the TMI-catalysed

*To whom correspondence should be addressed
†Massachusetts Institute of Technology
‡Now at: Swiss Federal Laboratories for Materials Science and Technology
¶Max Planck Institute for Chemistry
§IISER Mohali

oxidation pathway is underestimated by more than an order of magnitude in all current atmospheric chemistry models.

The three reactions showed an approximately mass-dependent relationship between ^{33}S and ^{34}S. However, the slope of the mass-dependent line was significantly different to 0.515 for the OH and TMI-catalysed pathways, reflecting kinetic versus equilibrium control of isotopic fractionation. For the TMI-catalysed pathway, both temperature dependence and $^{33}S/^{34}S$ relationship revealed a shift in the rate-limiting reaction step from dissolution at lower temperatures to TMI-sulfite complex formation at higher temperatures. 1D model results showed that although individual reactions could produce $\Delta^{33}S$ values between -0.15 and +0.2‰, seasonal changes in partitioning between oxidation pathways caused average sulfate $\Delta^{33}S$ values of 0‰ throughout the year.

1 Introduction

Sulfate and sulfur dioxide play an important role in environmental chemistry and climate through their effect on aerosol formation, size distribution and chemistry. The majority of anthropogenic and natural sulfur is released directly as SO_2 or oxidised to SO_2 in the atmosphere (*1–3*). Around 50% of global atmospheric sulfur dioxide is then oxidised to sulfate, while the rest is lost through dry and wet deposition (*4*, *5*). Sulfate aerosols have been shown to be responsible for cooling that has partially counteracted the effects of Greenhouse gas warming with a moderately high level of confidence (*6*), however the magnitude and expected future changes in sulfate aerosol radiative forcing remain one of the largest uncertainties associated with assessments of climate change (*7*).

The pathway by which SO_2 is oxidised to sulfate is critical in determining the radiative and environmental effects of SO_2 and sulfate. Gas-phase oxidation of SO_2 by OH radicals produces H_2SO_4 gas which can nucleate in the atmosphere to form new particles (*8*, *9*). These particles can have a strong impact on direct radiative forcing, and they can grow by the addition of organics and other compounds to eventually act as cloud condensation nuclei (CCN) (*9–11*) and increase the albedo and lifetime of clouds (*12*, *13*). Global model results attribute 17-36% of sulfate production

to this pathway (*5*, *14–16*). The rate of oxidation by this pathway is highest at the tropics, where $[O_3]$, humidity and insolation is highest (*17*).

Heterogeneous oxidation of SO_2 primarily occurs in cloud droplets, although oxidation on sea salt aerosols and mineral dust surfaces can be regionally important. The major aqueous-phase oxidants are H_2O_2, and O_2 catalysed by transition metal ions (TMIs) in a radical chain reaction pathway (*14*, *18–20*). While heterogeneous oxidation prevents H_2SO_4 gas production and thus new particle formation, it has other important climatic and environmental effects. In-cloud sulfate mass production modifies the aerosol size distribution, which affects both direct aerosol forcing, by significantly increasing the scattering efficiency of the particle population (*21*, *22*), and indirect aerosol forcing, by modifying the CCN activity of the particle population and potentially increasing the downwind CCN number concentration (*23*, *24*). Sulfate also acidifies particles, changing the bioavailability of many trace elements (*25*). Despite the importance of sulfate aerosol for climate, the partitioning between SO_2 oxidation pathways across different environments is poorly understood (*19*, *26*, *27*). Recent studies have shown that current models significantly underestimate the TMI catalysis pathway, which has significant implications for the radiative forcing (*19*, *27*). A detailed understanding of atmospheric sulfate formation pathways across different meteorological and chemical regimes is necessary to decrease the uncertainty in current climate assessments.

2 Stable isotopes of SO_2 and sulfate in the environment

Sulfur has four naturally-occurring stable isotopes, ^{32}S, ^{33}S, ^{34}S and ^{36}S, with natural abundances (*28*) of ∼95%, 0.75%, 4.2% and 0.015% respectively. The isotopic composition of a sulfur sample is described with the delta notation (expressed in permil):

$$\delta^x S = \frac{\left(\frac{n(^xS)}{n(^{32}S)}\right)_{\text{sample}}}{\left(\frac{n(^xS)}{n(^{32}S)}\right)_{\text{V-CDT}}} - 1 \quad (1)$$

where n is the number of atoms, ^{x}S is one of the heavy isotopes and V-CDT is the international sulfur isotope standard, Vienna Canyon Diablo Troilite.

Stable sulfur isotopes fractionate during reactions, so the isotopic composition of a product is not equal to the isotopic composition of the reactant. Fractionation factors can be characteristic for different reactions, and could be used to model and quantitatively assess the relative contributions of the major atmospheric SO_2 oxidation pathways on a regional and global scale. The kinetic isotope fractionation factor (α) is represented by the ratio of the heavy to the light isotope in the instantaneously-formed product divided by the ratio in the reactant:*

$$\alpha_x = \frac{\left(\frac{n(^{x}\mathrm{S})}{n(^{32}\mathrm{S})}\right)_{\text{products}}}{\left(\frac{n(^{x}\mathrm{S})}{n(^{32}\mathrm{S})}\right)_{\text{reactants}}} \tag{2}$$

When reaction extent is very low, α_{34} will directly reflect the different between reactant and product isotopic composition and the reactant isotopic composition will be essentially unchanged. However, as reaction extent increases in a closed or partially closed system such as an air parcel passing through a cloud (*19*), isotopic 'reservoir effects' will occur, where the isotopic composition of the reactant reservoir changes significantly. The isotopic composition of reactant and product as a function of reactant extent and fractionation factor is described by the Rayleigh fractionation equations (*29*, *30*), discussed further in Section S1.6 of the supplementary information. Values of α_{34} for oxidation of SO_2 by OH, H_2O_2 and transition metal ion catalysis (TMI-catalysis) have been recently reported (*31*, *32*), however the uncertainty in these results is relatively high (1-4‰) as isotope analyses were performed on extremely small sample sizes with NanoSIMS (Nanoscale Secondary Ion Mass Spectrometry). In particular, the temperature dependence of fractionation factors was smaller than the experimental error in these previous studies.

Fractionation in most reactions is 'mass-dependent', that is, the fractionation of ^{33}S has roughly half the magnitude of the fractionation of ^{34}S due to the relative mass differences between the

*The epsilon notation is also commonly used to indicate fractionation: $\varepsilon = (\alpha - 1) \times 1000$

isotopes (*33*). Mass-dependent fractionation is best described by the power law (*34–36*):

$$\alpha_{33} = (\alpha_{34})^{^{33}\theta} \tag{3}$$

where $^{33}\theta$ is an exponent describing relative fractionation of ^{33}S and ^{34}S. The defined value of $^{33}\theta$ is 0.515, which can be derived from theory of isotope fractionation (*33*) and also represents the average of the mass-dependent processes occurring on the Earth (*34*, *37*). The relationship between ^{33}S and ^{34}S is described in terms of the isotopic anomaly using this defined value of $^{33}\theta$ (*36*):

$$\Delta^{33}\mathrm{S} = 1000 \times [(\frac{\delta^{33}\mathrm{S}}{1000} + 1) - (\frac{\delta^{34}\mathrm{S}}{1000} + 1)^{0.515}] \tag{4}$$

Small deviations in $^{33}\theta$ of up to a few percent from 0.515 can occur in 'mass-dependent' processes, resulting in -0.2‰$< \Delta^{33}$S$<$0.2‰, while larger deviations are considered to be 'mass-independent' fractionation, resulting in an isotopic anomaly $>$0.2‰ in magnitude (*34–36*). The magnitude of the isotope anomaly therefore depends on both the exponent $^{33}\theta$ and the magnitude of α (*34–36*). Significant isotopic anomalies are very powerful tools for tracing reactions (*38*, *39*). Although the reactions considered in this paper are expected to be 'mass-dependent', small deviations in $^{33}\theta$ could produce non-zero values of Δ^{33}S which could act as an additional tracer for oxidation processes, complementary to the information gained from ^{34}S fractionation. Previous measurements of 33S fractionation during SO_2 oxidation are very uncertain (*31*), thus the $^{33}\theta$ values for the different reactions have not yet been reported.

The aim of this study is to improve the precision in known isotopic fractionation factors by measuring sulfur isotopic composition with isotope ratio mass spectrometry (IR-MS) following SO_2 oxidation by OH radicals, H_2O_2 and transition metal ion catalysis. The precision of results is sufficient to determine the $^{33}\theta$ values and the temperature dependence of fractionation factors for these three major atmospheric oxidation pathways, facilitating the use of sulfur isotopes to understand SO_2 oxidation in the ambient environment.

3 Materials and methods

3.1 Laboratory experiments

A brief description of the experiments will be given here; details can be found in the supplementary information. Gas phase oxidation was performed in a glass flow-through reactor with OH radicals generated from the photolysis of water. Aqueous oxidation experiments were performed in bubblers. For oxidation by H_2O_2, bubblers contained 1.5% or 6% solutions of H_2O_2, and for oxidation by TMI-catalysis, bubblers contained solutions of 10^{-5}-10^{-7} M Fe^{2+}/Fe^{3+} (previous studies have shown that the identity of the transition metal ion does not affect isotopic fractionation (*31*, *32*)). Following all experiments, sulfate was collected as $BaSO_4$ and reduced to Ag_2S (*40*, *41*) for measurement with isotope ratio mass spectrometry on a Thermo Electron MAT 253 instrument as described by Ono et al. (*36*). All results are corrected for blanks and reported relative to V-CDT. The fractionation factors were calculated from measured results using Rayleigh fractionation equations as described in the supplementary information.

3.2 Model study

A simple model was constructed to test if the measured fractionation factors can explain the seasonal isotopic composition of ambient sulfate (*39*, *42–44*). A brief description of the model is given here; full details are given in the supplementary material (Section S2.1-2.3). The model used the fractionation factors measured in this study to investigate seasonality in isotopic composition caused by i) seasonal changes in the fraction of SO_2 oxidised and ii) seasonal changes in fractionation factors due to temperature dependence.

We assumed that the SO_2 source flux was constant throughout the year and the source SO_2 had $\delta^{34}S$ and $\delta^{33}S = 0‰$, thus the results only show changes due to oxidation and not due to seasonality in emissions. This simplification means that the seasonal cycles in isotopic composition of SO_2 and sulfate alone are not relevant for comparison to observations. However, the difference between the isotopic composition of SO_2 and sulfate is a direct reflection of oxidation and removal processes

(aside from the marine boundary layer, where primary sea salt sulfate will make a significant contribution to atmospheric sulfate). Therefore, this can be directly compared to observations (see Figure 4).

Seasonality in the different oxidation pathways used in the model is shown in Figure 1 (*14*, *17*, *27*); consistent with recent results, the fraction of oxidation attributed to the TMI catalysis pathway was increased to 35% (of SO_2 oxidation, $\sim$15% of total SO_2 removal), to investigate the potential global importance of the pathway (*19*). This seasonality is applicable to continental areas in the northern mid-latitudes (45°N), where the dominant sources of anthropogenic SO_2 are located (*45*).

The model was run under three scenarios: 'full seasonality', where both the fraction oxidised and the fractionation factors (in response to temperature) vary through the year, 'constant F' where the fraction oxidised is constant throughout the year, and 'constant α' where the fractionation factor is set as the 0°C value throughout the year. 0°C was used as the temperature for the 'constant α' study for simplicity, as the temperature chosen affects only the magnitude and not the seasonality of fractionation. Oxidation of SO_2 by O_3 was not considered as the fractionation factor is not well-constrained, however this pathway is self-limiting due to pH and contributes only a minor proportion of annual average oxidation (*4*, *14*, *46*). The calculations used in the seasonality model are described in detail in Section S2 of the supplementary information.

4 Results

4.1 Fractionation of ^{34}S during oxidation reactions

The measured α values are shown in Table 1 and Figure 2. The temperature dependence of the isotopic fractionation factors was determined with weighted linear regression of all the measurement points shown in Figure 2; in addition to the four new measurements of the gas-phase fractionation factor for oxidation by OH, the four previous measurements at -25, 0, 19 and 40°C from Harris et al. (*31*) were used in the regression. The temperature-dependent regression line for the

fractionation factor for oxidation of SO_2 by OH radicals in the gas phase is (expressed in permil):

$$\alpha_{34} - 1\ (‰) = (10.60 \pm 0.73) - (0.004 \pm 0.015) \cdot \mathrm{T} \tag{5}$$

where T is the temperature in °C. The IR-MS value at 11.4°C and the NanoSIMS value at 38°C fall above and below the regression line respectively, although both values agree within the 2σ error (Figure 2). At lower reaction temperatures where absolute humidity and thus OH concentration is lower, NanoSIMS results should be better than IR-MS results, as the NanoSIMS requires very little product, thus the isotopic composition of both the residual SO_2 and product sulfate can be measured. At higher temperatures the quantity of OH and therefore of product sulfate is higher, so high-precision IR-MS results are preferable to the low-precision NanoSIMS results. The combination of the two datasets reveals that isotopic fractionation of SO_2 by OH is insensitive to temperature over the range of temperatures encountered in the present-day lower troposphere.

Fractionation during SO_2 dissolution and aqueous phase oxidation has been measured in several studies (*31*, *47–49*) (shown together with the new results in Figure 2). The temperature dependence of sulfur isotope fractionation during aqueous phase oxidation by H_2O_2 was found from regression of all points in Figure 2 to be:

$$\alpha_{34,H_2O_2} - 1\ (‰) = (16.51 \pm 0.15) - (0.085 \pm 0.004) \cdot \mathrm{T} \tag{6}$$

The new results agree well with the results of Harris et al. (*31*) and the higher-temperature results from Egiazarov et al. (*47*). The results of Eriksen et al. (*48*, *49*) are systematically lower than all other results, which may be due to the low pH at which the experiments were performed, as sulfur isotope fractionation increases with pH by around 5‰ from pH 2 to pH 7 (*50*). The combined results show that the temperature dependence of isotopic fractionation during oxidation by H_2O_2 is significant at the 99% confidence level.

Unlike oxidation of SO_2 by H_2O_2 and OH radicals, the light isotope is favoured in oxidation of SO_2 by the TMI catalysis pathway. The new and previous (*32*) measurements of fractionation

during oxidation by TMI catalysis at ∼19°C (-9.70±0.04‰ and -9.5±3.1‰ respectively) agree very well. The ^{34}S fractionation factor (from all points in Figure 2) for oxidation of SO_2 via TMI catalysis is:

$$\alpha_{34,TMI} - 1\ (‰) = (-5.039 \pm 0.044) - (0.237 \pm 0.004) \cdot \mathrm{T} \quad (7)$$

This is the first measurement of the temperature dependence of isotope fractionation during oxidation by the TMI catalysis pathway. Unlike the H_2O_2 oxidation pathway, the TMI catalysis pathway shows an inverse temperature dependence, where the fractionation factor becomes larger with increasing temperature. The magnitude of the temperature effect is more than twice as large for TMI-catalysed oxidation as for oxidation by H_2O_2, and will cause a very significant isotopic effect (up to 20‰) with spatial and temporal variations in temperature.

4.2 Mass-dependence of fractionation during oxidation

To determine $^{33}\theta$ values for the three reactions, α_{33} values were first calculated for each experiment. α_{33} values were calculated with Rayleigh equations as described in the supplementary material (S1.6) for α_{34}, however the values of f_{rem} were not recalculated from ^{33}S results; f_{rem} values from ^{34}S mass balance given in Table 1 were used. Following equation 3, the natural logarithms of α_{33} and α_{34} were plotted against each other to calculate the value of θ_{33} (Figure 3). Linear regressions were weighted by error in both $\ln(\alpha_{34})$ and $\ln(\alpha_{33})$ (*51*, *52*) and forced through 0 to find the values of θ_{33} and the 1σ error for the three oxidants (see Figure 3 and Table 2). For oxidation by the OH radical, θ_{33} was less than 0.515, while for oxidation by H_2O_2 the measured θ_{33} agreed with the expected value of 0.515 (*34*, *37*). For the lower temperature TMI-catalysis experiments, θ_{33} was < 0.515 while for the higher-temperature experiments θ_{33} was > 0.515.

5 Discussion

5.1 Temperature dependence of isotope fractionation

The expected temperature dependence in isotopic fractionation is a reduction in the magnitude of fractionation with increasing temperature, as the energy differences between isotopes are less important relative to the increased energy of the whole system at higher temperatures (*30*). This is seen for oxidation by H_2O_2, however the fractionation during oxidation by TMI catalysis becomes significantly larger in magnitude with increased temperature, over the measured temperature range of 0 to 25°C. A possible explanation is that the rate-limiting step changes with temperature:

- At low temperatures, the rate of SO_2 exchange between gaseous and aqueous phases is decreased, thus dissolution becomes the rate-limiting step of the reaction and is able to have an effect on isotopic fractionation. As shown previously (*31*, *50*) and supported by the H_2O_2 fractionation factor from this study, dissolution results in $\alpha > 1$. It would therefore be expected that at temperatures lower than the range measured in this study, the fractionation factor for TMI-catalysed oxidation may be >1.

- At higher temperatures, dissolution is rapid and the catalytic chain reaction is rate-limiting, resulting in strong kinetic fractionation favouring the light isotope. It is expected that the magnitude of kinetic fractionation associated with this reaction will decrease with increasing temperature. Thus, at a temperature higher than the measured range (ie. >>25°C the magnitude of fractionation is predicted to decrease and eventually approach zero at very high temperatures.

Further measurements over a larger range of temperatures would be useful to fully constrain the TMI catalysis fractionation factor, particularly at lower temperatures which are often observed in clouds (*53*).

5.2 Seasonality in sulfate isotopic composition

A number of studies have observed seasonality in the isotopic composition of SO_2 and sulfate, and several possible causes have been proposed for this seasonality: seasonality in isotopic composition of emitted SO_2 (*42*, *54–56*), seasonal changes in the contribution of isotopically heavy sea salt sulfate (*57*, *58*), seasonally-changing fractionation factors due to temperature-dependence (*59*), and seasonal changes in partitioning between oxidation pathways (*42–44*). A simple model based on the isotopic fractionation factors measured in this study can isolate and constrain the possible effect of temperature dependence in fractionation factors and seasonal changes in partitioning on SO_2 and sulfate isotopic composition. Figure S3 in the supplementary material shows the seasonal isotopic composition of SO_2 and sulfate for the three scenarios described in Section 3.2; this does not account for seasonality in emitted SO_2 and is therefore not directly comparable to observations.

The three scenarios show the influence of different factors on the strength of seasonality in isotopic composition with respect to each oxidation pathway. For oxidation by OH radicals, temperature dependence of the fractionation factor is insignificant (0.004 ± 0.015 ‰ $^{\circ}C^{-1}$, see Section 4.1) and therefore only seasonal changes in the proportion of SO_2 oxidised by this pathway cause seasonality in isotopic composition of sulfate produced by this pathway relative to SO_2. The OH pathway has the strongest reservoir effects, with the SO_2 isotopic composition depleted by nearly 3‰ in summer due to preferential oxidation of the heavy isotope (see Figure S3, top right hand panel); oxidation by OH is concentrated into the daylight hours, making the proportion of SO_2 oxidised higher and thus the reservoir effects much stronger than for the other pathways. For TMI catalysis, the total fraction of SO_2 removed is never >0.25, thus enrichment of ^{34}S in the reservoir is <1‰, and only temperature dependence in the fractionation factor (0.237 ± 0.004 ‰ $^{\circ}C^{-1}$) causes seasonality. The isotopic composition of SO_2 and sulfate relative to the H_2O_2 oxidation pathway shows no seasonality as neither the fraction reacted nor the temperature dependence (0.085 ± 0.004 ‰ $^{\circ}C^{-1}$; $\sim 3\times$ smaller than for TMI-catalysed oxidation) are large enough to be significant for seasonality.

In the ambient environment, the isotopic composition of SO_2 and sulfate depends on the emitted

SO_2, while the difference between the isotopic composition of SO_2 and sulfate depends only on oxidation, transport and removal. Figure 4 therefore shows the modelled difference in $\delta^{34}S$ of SO_2 and sulfate compared to several studies (*42–44*). The seasonality in the constant α scenario (Figure 4b) is $\sim$2.5$\times$ stronger than in the constant F scenario (Figure 4c), showing that reservoir effects due to partitioning between oxidation pathways are the dominant overall cause of seasonality in $\delta^{34}S$.

Comparison to observations (Figure 4a) shows that attributing 35% of SO_2 oxidation (15% of total SO_2 removal) to the TMI-catalysis pathway in the northern hemisphere mid-latitudes - as was done in this model - may be conservative. The model results for the first half of the year agree very well with measurements made between 1993 and 1996 in the Czech Republic (*42*), however for the second half of the year the measurements are significantly lower than the model results. This could either be due to underestimation of the TMI-catalysis pathway or underestimation of the reservoir effect. For August-October, the fraction of SO_2 removed by oxidation (as opposed to wet or dry deposition) would need to be $>$90% to agree with isotopic observations, which is not in agreement with observations of the SO_2:sulfate ratio (*43*, *44*) or models of the sulfur cycle (*5*, *27*, *60*), thus it appears the TMI-catalysis pathway is underestimated by 10-30% during these months. A similar pattern is seen for samples taken in 1980 in New Hampshire (*44*), although these earlier results show an even lower difference between $\delta^{34}S$ of SO_2 and sulfate, requiring that TMI-catalysed oxidation contributes $>$40-50% of oxidation (15-25% of total SO_2 removal). Measurements from 1997 at coastal and continental sites in China (*43*) show similar seasonality, although scatter is large.

The results from China confirm that 35% TMI-catalysed oxidation is an underestimation; all points fall within or below the lower limit of the model values, which can only be explained at continental sites by an underestimation of the TMI-catalysis pathway. For continental Chinese sites, this is expected given the high dust loading these locations would experience particularly in winter, leading to increased importance of the TMI-catalysis pathway during winter. While European and North American sites may show high levels of TMIs in winter due to increased

power generation and emissions, recent results have shown that natural TMIs are likely to be much stronger catalysts of SO_2 oxidation than anthropogenic TMIs (*19*). At coastal Chinese sites, observations below the modelled line may also point to the importance of oxidation by HOCl and HOBr (*61–63*); this pathway has $\alpha < 1$ (*50*) and its importance in the marine boundary layer is not well-quantified (*61*, *64*, *65*). Little or no seasonality occurs in the Chinese data. This is not reflected in the model, which does not consider seasonality in factors such as sea spray, oceanic biogenic SO_2 and dust emission that may play a very important role in seasonality of the sulfur cycle in these regions. These estimates provide a first guess to consider the importance of these three oxidation pathways in terms of $\delta^{34}S$ observations; more observations with a wider range of spatial and temporal coverage in combination with a sophisticated chemistry-transport model such as GEOS-Chem would be the next step to gain a more quantitative understanding of sulfur oxidation pathways.

In summary, seasonal changes in reservoir effects and partitioning of oxidation pathways was the most important cause of seasonality in isotopic composition. The comparison of measured fractionation factors in a simple model with observations confirms that the TMI-catalysis pathway is strongly underestimated in the northern hemisphere mid-latitudes, where the majority of anthropogenic SO_2 sources are located (*45*). Alexander et al. (*27*) predicted this pathway may be particularly important in high latitude winters, but estimated it contributes only 9-17% of SO_2 oxidation (>10% of SO_2 removal) globally. We estimate that the pathway contributes >35% of SO_2 oxidation (>15% of SO_2 removal) in the northern hemisphere with a strong latitudinal dependence based on the availability of natural dust TMIs and other oxidants. Further investigation in the field and with model studies, particularly in the Southern Hemisphere and in tropical regions, is needed to refine this number and estimate spatial variations; however, it is clear that this pathway is underestimated by more than an order of magnitude in all current models, with implications for estimates of sulfate environmental and climatic effects (see (*19*) for a summary of sulfur models). The fractionation factors measured in this study, in combination with models and seasonal field measurements, are a powerful tool to understand partitioning between SO_2 oxidation pathways, in

particular the global importance of different oxidation pathways.

5.3 Mass-dependence of isotopic fractionation

The values of $^{33}\theta$ are significantly different to 0.515 for oxidation by OH and TMI-catalysis, but not for oxidation by H_2O_2. These reactions are still described as 'mass dependent', as the values of $^{33}\theta$ deviate by only a few percent from expected mass dependent fractionation. It is expected that $^{33}\theta$ for equilibrium processes is very close to 0.515, as described by partition function ratios reflecting zero point energy differences, while for kinetic processes it may be closer to 0.5 as described by transition state theory (*66*, *67*). This is in agreement with the results of this study: For the OH reaction, the measured $^{33}\theta$ (0.503) reflects kinetic fractionation while for H_2O_2 (0.511) fractionation is primarily controlled by acid-base equilibria (*50*).

The results for TMI-catalysed oxidation are more complex. It appears that there is a change in the reaction controlling isotopic fractionation (i.e. the rate-limiting step of the reaction) between 17.1 and 23.5°C. At lower temperatures $^{33}\theta$ (0.498) suggests kinetic control while at higher temperatures $^{33}\theta$ (0.537) may reflect equilibrium processes, although it is significantly $>$0.515. This is consistent with the observed temperature dependence, which also showed a shift in the rate-limiting reaction step with temperature. The results show that kinetically-controlled dissolution is rate-limiting at lower temperatures, while at higher temperatures an equilbrium associated with the catalytic chain reaction limits reaction rate. Berglund et al. (*68*) proposed that this chain reaction begins with the reversible formation of a complex between the catalytic TMI and hydrogen sulfite, eg. $MnHSO_3^+$; the remaining steps of the chain reaction are irreversible and would therefore be more likely to produce $^{33}\theta \approx 0.5$. This result may be an important consideration when the rate of TMI-catalysed oxidation is considered in models.

Although the reactions considered in this study are essentially mass-dependent, small isotopic anomalies $< 0.2‰$ will still result when $^{33}\theta \neq 0.515$. Figure 5 shows the expected $\Delta^{33}S$ values for atmospheric sulfate predicted over a year. The magnitude of $\Delta^{33}S$ from the OH reaction peaks in winter when reacted fraction is lowest and reservoir effects are negligible; similarly, $\Delta^{33}S$ for the

TMI-catalysed reaction peaks in summer. The small dip in $\Delta^{33}S$ for TMI-catalysed oxidation is due to the shift from 'low' temperature ($^{33}\theta < 0.515$) to 'high' temperature ($^{33}\theta > 0.515$) regimes; this dip is not significant compared to the uncertainty, and may be an artefact as the exact shape of temperature dependence of $^{33}\theta$ between 0 and 25°C is not known. Although $\Delta^{33}S$ of sulfate with respect to the individual reactions is significantly different from 0‰ for oxidation by OH and TMI-catalysis, when the three pathways are combined opposing seasonalities result in $\Delta^{33}S \approx$ 0‰ throughout the year. This is in agreement with the majority of ambient observations, which generally show no ^{33}S isotope anomaly in tropospheric aerosol; the modelled results agree within the uncertainty with seasonal measurements of tropospheric background aerosol from Antarctic ice cores (*39*).

Measurements of $\Delta^{33}S$ on a local scale may prove useful to differentiate between OH and H_2O_2 oxidation, which are poorly resolved using $\delta^{34}S$ measurements. For example, diurnally-resolved measurements of $\delta^{34}S$ and $\Delta^{33}S$ in aerosol could be used to conduct a multivariate analysis to constrain partitioning between oxidation pathways with much less uncertainty than either measurement alone. In addition, $\Delta^{33}S$ values >0.5‰ have been recently observed (*38*, *69*). The results of this study suggest that the MIF observed in tropospheric sulfate aerosol could potentially arise from a very strong reservoir effect causing $\Delta^{33}S > 0.5$‰ in SO_2 followed by MDF-oxidation to sulfate conserving the MIF imprint from the SO_2. Alternatively, MIF in tropospheric aerosol could arise from the mixing or entrainment of stratospheric air, which can have significant $\Delta^{33}S$ values arising from UV photoexcitation of SO_2 leading to sulfate production at high column densities of SO_2 eg. following volcanoes (*70*, *71*).

The other possibility is that an SO_2 oxidation pathway not considered in this study causes significant MIF; for example, oxidation by hypohalites such as OCl or OBr or Cl radicals (*61*, *65*). Oxidation by O_3 is very unlikely to produce MIF, as previous laboratory results showed that fractionation is controlled by dissolution in a similar manner to H_2O_2 oxidation (*31*, *50*). Oxidation by Cl radicals is likely to initiate a radical chain reaction and may produce isotopic fractionation similar to TMI-catalysed oxidation. Recently, H_2SO_4 (g) production by Criegee

radicals or ionising radiation have been recognised as non-traditional but potentially important and underestimated SO_2 oxidation pathways (*72*, *73*); the $\Delta^{33}S$ effect produced by these pathways may be significant, and should be considered when quantifying sulfate production pathways from $\Delta^{33}S$ measurements. A combination of $\Delta^{33}S$ and $\delta^{34}S$ measurements in the field and laboratory are needed to fully understand the role of various oxidation pathways in the environment. However, the relatively good agreement between observed and modelled values of $\Delta^{33}S$ and $\delta^{34}S$ suggests that the three pathways considered in this study explain the majority of SO_2 oxidation in the northern hemisphere mid-latitudes.

Acknowledgments

We thank Katherine Thomas and Bill Olszewski for assistance with laboratory work and isotopic measurements, and Anke Nölscher and Vinayak Sinha for measurements of OH concentration. The Teflon FEP 121a suspension used to coat the OH radical reactor was kindly provided by DuPont. This research was funded by the Max Planck Society and the Max Planck Graduate Centre.

The supplementary information file contains details regarding the experimental methods (Section 1) and model calculations (Section 2) as well as Figures S1-S3 and Tables S1-S2. This information is available free of charge via the Internet at http://pubs.acs.org/

Word count:

- Word count (as estimated by ES&T) before revision, including figures and tables: 5890
- 1041 words added in response to review comments
- Estimated current word count = 6931 words.

References

(1) Berresheim, H.; Wine, P. H.; Davis, D. In *Composition, Chemistry and Climate of the Atmosphere*; Singh, H., Ed.; Van Nostrand Reinhold, USA, 1995; pp 251–307.

(2) Berresheim, H.; Elste, T.; Tremmel, H. G.; Allen, A. G.; Hansson, H. C.; Rosman, K.; Dal Maso, M.; Makela, J. M.; Kulmala, M.; O'Dowd, C. D. Gas-aerosol relationships of H_2SO_4, MSA, and OH: Observations in the coastal marine boundary layer at Mace Head, Ireland. *Journal of Geophysical Research - Atmospheres* **2002**, *107*, D19.

(3) Seinfeld, J. H.; Pandis, S. N. *Atmospheric Chemistry and Physics*; Wiley & Sons: New York, 1998.

(4) Chin, M.; Jacob, D. J.; Gardner, G. M.; ForemanFowler, M. S.; Spiro, P. A.; Savoie, D. L. A global three-dimensional model of tropospheric sulfate. *Journal of Geophysical Research - Atmospheres* **1996**, *101*, 18667–18690.

(5) Chin, M.; Savoie, D. L.; Huebert, B. J.; Bandy, A. R.; Thornton, D. C.; Bates, T. S.; Quinn, P. K.; Saltzman, E. S.; De Bruyn, W. J. Atmospheric sulfur cycle simulated in the global model GOCART: Comparison with field observations and regional budgets. *Journal of Geophysical Research - Atmospheres* **2000**, *105*, 24689–24712.

(6) Denman, K. In *Climate Change 2007: The physical science basis. Contribution of the working group I to the Fourth Assessment Report of the Intergovernmental Panel on Climate Change.*; Solomon, S., Ed.; Cambridge University Press, New York, 2007.

(7) Solomon, S. In *Climate Change 2007: The physical science basis. Contribution of the working group I to the Fourth Assessment Report of the Intergovernmental Panel on Climate Change.*; Solomon, S., Ed.; Cambridge University Press, New York, 2007.

(8) Tanaka, N.; Rye, D. M.; Xiao, Y.; Lasaga, A. C. Use of Stable Sulfur Isotope Systematics for

Evaluating Oxidation Reaction Pathways and in-Cloud Scavenging of Sulfur-Dioxide in the Atmosphere. *Geophysical Research Letters* **1994**, *21*, 1519–1522.

(9) Kulmala, M.; Vehkamaki, H.; Petaja, T.; Maso, M. D.; Lauri, A.; Kerminen, V. M.; Birmili, W.; McMurry, P. H. Formation and growth rates of ultrafine atmospheric particles: a review of observations. *Journal of Aerosol Science* **2004**, *35*, 143–176.

(10) Kulmala, M. et al. Toward direct measurement of atmospheric nucleation. *Science* **2007**, *318*, 89–92.

(11) Benson, D. R.; Young, L. H.; Kameel, F. R.; Lee, S. H. Laboratory-measured nucleation rates of sulfuric acid and water binary homogeneous nucleation from the SO2 + OH reaction. *Geophysical Research Letters* **2008**, *35*, L11801.

(12) Twomey, S. Aerosol, Clouds and Radiation. *Atmospheric Environment* **1991**, *25A*, 2435–2442.

(13) Boucher, O.; Lohmann, U. The sulfate-CCN-cloud albedo effect: A sensitivity study with two general circulation models. *Tellus* **1995**, *47B*, 281–300.

(14) Sofen, E.; Alexander, B.; Kunasek, S. A. The impact of anthropogenic emissions on atmospheric sulfate production pathways, oxidants and ice core Delta17O(sulfate). *Atmospheric Chemistry and Physics* **2011**, *11*, 3565–3578.

(15) Berglen, T.; Berntsen, T.; Isaksen, I.; Sundet, J. A global model of the coupled sulfur/oxidant chemistry in the troposphere: The sulfur cycle. *Journal of Geophysical Research - Atmospheres* **2004**, *109*, D19310.

(16) Pozzoli, L.; Bey, I.; Rast, S.; Schultz, M. G.; Stier, P.; Feichter, J. Trace gas and aerosol interactions in the fully coupled model of aerosol-chemistry-climate ECHAM5-HAMMOZ: 1. Model description and insights from the spring 2001 TRACE-P experiment. *Journal of Geophysical Research - Atmospheres* **2008**, *113*, D07308–.

(17) Bahm, K.; Khalil, M. A new model of tropospheric hydroxyl radical concentrations. *Chemosphere* **2004**, *54*, 143–166.

(18) Herrmann, H.; Ervens, B.; Jacobi, H. W.; Wolke, R.; Nowacki, P.; Zellner, R. CAPRAM2.3: A chemical aqueous phase radical mechanism for tropospheric chemistry. *Journal of Atmospheric Chemistry* **2000**, *36*, 231–284.

(19) Harris, E. et al. Enhanced role of transition metal ion catalysis during in-cloud oxidation of SO2. *Science* **2013**, *340*, 727–730.

(20) Rotstayn, L.; Lohmann, U. Simulation of the tropospheric sulfur cycle in a global model with a physically based cloud scheme. *Journal of Geophysical Research - Atmospheres* **2002**, *107*, 4592.

(21) Hegg, D. A.; Covert, D. S.; Jonsson, H.; Khelif, D.; Friehe, C. A. Observations of the impact of cloud processing on aerosol light-scattering efficiency. *Tellus Series B: Chemical and Physical Meteorology* **2004**, *56*, 285–293.

(22) Yuskiewicz, B. A.; Stratmann, F.; Birmili, W.; Wiedensohler, A.; Swietlicki, E.; Berg, O.; Zhou, J. The effects of in-cloud mass production on atmospheric light scatter. *Atmospheric Research* **1999**, *50*, 265–288.

(23) Mertes, S.; Galgon, D.; Schwirn, K.; Nowak, A.; Lehmann, K.; Massling, A.; Wiedensohler, A.; Wieprecht, W. Evolution of particle concentration and size distribution observed upwind, inside and downwind hill cap clouds at connected flow conditions during FEBUKO. *Atmospheric Environment* **2005**, *39*, 4233–4245.

(24) Mertes, S.; Lehmann, K.; Nowak, A.; Massling, A.; Wiedensohler, A. Link between aerosol hygroscopic growth and droplet activation observed for hill-capped clouds at connected flow conditions during FEBUKO. *Atmospheric Environment* **2005**, *39*, 4247–4256.

(25) Jickells, T. D. et al. Global iron connections between desert dust, ocean biogeochemistry, and climate. *Science* **2005**, *308*, 67–71.

(26) Barrie, L. A. et al. A comparison of large-scale atmospheric sulphate aerosol models (COSAM): overview and highlights. *Tellus Series B: Chemical and Physical Meteorology* **2001**, *53*, 615–645.

(27) Alexander, B.; Park, R. J.; Jacob, D. J.; Gong, S. L. Transition metal-catalyzed oxidation of atmospheric sulfur: Global implications for the sulfur budget. *Journal of Geophysical Research-Atmospheres* **2009**, *114*, D02309.

(28) Ding, T.; Valkiers, S.; Kipphardt, H.; De Bievre, P.; Taylor, P. D. P.; Gonfiantini, R.; Krouse, R. Calibrated sulfur isotope abundance ratios of three IAEA sulfur isotope reference materials and V-CDT with a reassessment of the atomic weight of sulfur. *Geochimica Et Cosmochimica Acta* **2001**, *65*, 2433–2437.

(29) Mariotti, A.; Germon, J. C.; Hubert, P.; Kaiser, P.; Letolle, R.; Tardieux, A.; Tardieux, P. Experimental-determination of Nitrogen Kinetic Isotope Fractionation - Some Principles - Illustration For the Denitrification and Nitrification Processes. *Plant and Soil* **1981**, *62*, 413–430.

(30) Krouse, H. R.; Grinenko, V. A. *Stable isotopes: Natural and anthropogenic sulphur in the environments*; Wiley: Chichester, 1991; Vol. 43.

(31) Harris, E.; Sinha, B.; Hoppe, P.; Crowley, J. N.; Ono, S.; Foley, S. Sulfur isotope fractionation during oxidation of sulfur dioxide: Gas-phase oxidation by OH radicals and aqueous oxidation by H2O2, O3 and iron catalysis. *Atmospheric Chemistry and Physics* **2012**, *12*, 407–423.

(32) Harris, E.; Sinha, B.; Foley, S.; Crowley, J. N.; Borrmann, S.; Hoppe, P. Sulfur isotope fractionation during heterogeneous oxidation of SO2 on mineral dust. *Atmospheric Chemistry and Physics* **2012**, *12*, 4867–4884.

(33) Urey, H. The thermodynamic properties of isotopic substances. *Journal of the Chemical Society* **1947**, 562–581.

(34) Farquhar, J.; Wing, B. A. Multiple sulfur isotopes and the evolution of the atmosphere. *Earth and Planetary Science Letters* **2003**, *213*, 1–13.

(35) Farquhar, J.; Johnston, D. T.; Wing, B. A.; Habicht, K. S.; Canfield, D. E.; Airieau, S.; Thiemens, M. H. Multiple sulphur isotopic interpretations of biosynthetic pathways: implications for biological signatures in the sulphur isotope record. *Geobiology* **2003**, *1*, 27–36.

(36) Ono, S.; Wing, B.; Johnston, D.; Farquhar, J.; Rumble, D. Mass-dependent fractionation of quadruple stable sulfur isotope system as a new tracer of sulfur biogeochemical cycles. *Geochimica et Cosmochimica Acta* **2006**, *70*, 2238–2252.

(37) Hulston, J. R.; Thode, H. G. Variations in the S33, S34, and S36 Contents of Meteorites and Their Relation to Chemical and Nuclear Effects. *Journal of Geophysical Research* **1965**, *70*, 3475–3484.

(38) Romero, A. B.; Thiemens, M. H. Mass-independent sulfur isotopic compositions in present-day sulfate aerosols. *Journal of Geophysical Research - Atmospheres* **2003**, *108*, AAC8–1–7.

(39) Savarino, J.; Romero, A.; Cole-Dai, J.; Bekki, S.; Thiemens, M. H. UV induced mass-independent sulfur isotope fractionation in stratospheric volcanic sulfate. *Geophysical Research Letters* **2003**, *30*, 2131.

(40) Thode, H. G.; Monster, J.; Dunford, H. B. Sulphur Isotope Geochemistry. *Geochimica Et Cosmochimica Acta* **1961**, *25*, 159–174.

(41) Forrest, J.; Newman, L. Ag-110 Microgram Sulfate Analysis For Short Time Resolution of Ambient Levels of Sulfur Aerosol. *Analytical Chemistry* **1977**, *49*, 1579–1584.

(42) Novak, M.; Jackova, I.; Prechova, E. Temporal Trends in the Isotope Signature of Air-Borne Sulfur in Central Europe. *Environmental Science & Technology* **2001**, *35*, 255–260.

(43) Mukai, H.; Tanaka, A.; Fujii, T.; Zeng, Y. Q.; Hong, Y. T.; Tang, J.; Guo, S.; Xue, H. S.; Sun, Z. L.; Zhou, J. T.; Xue, D. M.; Zhao, J.; Zhai, G. H.; Gu, J. L.; Zhai, P. Y. Regional characteristics of sulfur and lead isotope ratios in the atmosphere at several Chinese urban sites. *Environmental Science & Technology* **2001**, *35*, 1064–1071.

(44) Saltzman, E. S.; Brass, G.; Price, D. The mechanism of sulfate aerosol formation: Chemical and sulfur isotopic evidence. *Geophysical Research Letters* **1983**, *10*, 513–516.

(45) NASA, Multi-Decadal Sulfur Dioxide Climatology from Satellite Instruments. 2013; `http://so2.gsfc.nasa.gov/`.

(46) Botha, C. F.; Hahn, J.; Pienaar, J. J.; Vaneldik, R. Kinetics and mechanism of the oxidation of sulfur(IV) by ozone in aqueous solutions. *Atmospheric Environment* **1994**, *28*, 3207–3212.

(47) Egiazarov, A. C.; Kaviladze, M.; Kerner, M. N.; Oziashvili, E. L.; Ebralidze, A.; Esakiya, A. D. Separation of Sulfur Isotopes by Chemical Exchange. *Isotopenpraxis: Isotopes in Environmental and Health Studies* **1971**, *7*, 379–383.

(48) Eriksen, T. E. Sulfur Isotope Effects 1. Isotopic Exchange Coefficient for Sulfur Isotopes 34S-32S in System SO2(g)-HSO3(aq) at 25, 35, and 45 Degrees C. *Acta Chemica Scandinavica* **1972**, *26*, 573–580.

(49) Eriksen, T. E. Sulfur Isotope Effects 4. Sulfur Isotope Effects in Anion-Exchange Systems. *Acta Chemica Scandinavica* **1972**, *26*, 980.

(50) Harris, E.; Sinha, B.; Hoppe, P.; Foley, S.; Borrmann, S. Fractionation of sulfur isotopes during heterogeneous oxidation of SO2 on sea salt aerosol: A new tool to investigate non-sea salt sulfate production in the marine boundary layers. *Atmospheric Chemistry and Physics* **2012**, *12*, 4619–4631.

(51) Wiens, T. Linear Regression with Errors in X and Y [Software]. 2010; `http://www.mathworks.com/matlabcentral/fileexchange/26586`.

(52) York, D.; Evensen, N.; Martinez, M.; De Basabe Delgado, J. Unified equations for the slope, intercept and standard errors of the best straight line. *American Journal of Physics* **2004**, *72*, 367–375.

(53) Rosenfeld, D.; Woodley, W. L. Deep convective clouds with sustained supercooled liquid water down to-37.5 degrees C. *Nature* **2000**, *405*, 440–442.

(54) Nriagu, J. O.; Coker, R. D. Isotopic Composition of Sulfur in Atmospheric Precipitation around Sudbury, Ontario. *Nature* **1978**, *274*, 883–885.

(55) Nriagu, J. O.; Coker, R. D. Isotopic Composition of Sulfur in Precipitation within the Great Lakes Basin. *Tellus* **1978**, *30*, 365–375.

(56) Mayer, B.; Feger, K. H.; Giesemann, A.; Jaeger, H. J. Interpretation of sulfur cycling in two catchments in the Black Forest (Germany) using stable sulfur and oxygen isotope data. *Biogeochemistry* **1995**, *30*, 31–58.

(57) Ohizumi, T.; Fukuzaki, N.; Kusakabe, M. Sulfur isotopic view on the sources of sulfur in atmospheric fallout along the coast of the Sea of Japan. *Atmospheric Environment* **1997**, *31*, 1339–1348.

(58) Ohizumi, T.; Take, N.; Moriyama, N.; Suzuki, O.; Kusakabe, M. Seasonal and spatial variations in the chemical and sulfur isotopic composition of acid deposition in Niigata Prefecture, Japan. *Water Air and Soil Pollution* **2001**, *131*, 1679–1684.

(59) Caron, F.; Tessier, A.; Kramer, J. R.; Schwarcz, H. P.; Rees, C. E. Sulfur and oxygen isotopes of sulfate in precipitation and lakewater, Quebec, Canada. *Applied Geochemistry* **1986**, *1*, 601–606.

(60) Faloona, I.; Conley, S. A.; Blomquist, B.; Clarke, A. D.; Kapustin, V.; Howell, S.; Lenschow, D. H.; Bandy, A. R. Sulfur dioxide in the tropical marine boundary layer: dry

deposition and heterogeneous oxidation observed during the Pacific Atmospheric Sulfur Experiment. *Journal of Atmospheric Chemistry* **2009**, *63*, 13–32.

(61) von Glasow, R.; Sander, R.; Bott, A.; Crutzen, P. J. Modeling halogen chemistry in the marine boundary layer - 2. Interactions with sulfur and the cloud-covered MBL. *Journal of Geophysical Research - Atmospheres* **2002**, *107*, D17.

(62) Troy, R. C.; Margerum, D. W. Nonmetal Redox Kinetics - Hypobromite and Hypobromous Acid Reactions With Iodide and With Sulfite and the Hydrolysis of Bromosulfate. *Inorganic Chemistry* **1991**, *30*, 3538–3543.

(63) Yiin, B. S.; Margerum, D. W. Kinetics of Hydrolysis of the Chlorosulfate Ion. *Inorganic Chemistry* **1988**, *27*, 1670–1672.

(64) Shaka, H.; Robertson, W. H.; Finlayson-Pitts, B. J. A new approach to studying aqueous reactions using diffuse reflectance infrared Fourier transform spectrometry: application to the uptake and oxidation of SO2 on OH-processed model sea salt aerosol. *Physical Chemistry Chemical Physics* **2007**, *9*, 1980–1990.

(65) Hoppel, W. A.; Caffrey, P. F. Oxidation of S(IV) in sea-salt aerosol at high pH: Ozone versus aerobic reaction. *Journal of Geophysical Research - Atmospheres* **2005**, *110*, D23202.

(66) Young, E. D.; Galy, A.; Nagahara, H. Kinetic and equilibrium mass-dependent isotope fractionation laws in nature and their geochemical and cosmochemical significance. *Geochimica Et Cosmochimica Acta* **2002**, *66*, PII S0016–7037(01)00832–8.

(67) Bigeleisen, J. The relative velocities of isotopic molecules. *Journal of Chemical Physics* **1949**, *15*, 261–267.

(68) Berglund, J.; Fronaeus, S.; Elding, L. I. Kinetics and Mechanism For Manganese-catalyzed Oxidation of Sulfur(iv) By Oxygen In Aqueous-solution. *Inorganic Chemistry* **1993**, *32*, 4527–4538.

(69) Guo, Z. B.; Li, Z. Q.; Farquhar, J.; Kaufman, A. J.; Wu, N. P.; Li, C.; Dickerson, R. R.; Wang, P. C. Identification of sources and formation processes of atmospheric sulfate by sulfur isotope and scanning electron microscope measurements. *Journal of Geophysical Research-atmospheres* **2010**, *115*.

(70) Hattori, S.; Schmidt, J. A.; Johnson, M. S.; Danielache, S. O.; Yamada, A.; Ueno, Y.; Yoshida, N. SO2 photoexcitation mechanism links mass-independent sulfur isotopic fractionation in cryospheric sulfate to climate impacting volcanism. *Proceedings of the National Academy of Sciences* **2013**, –.

(71) Baroni, M.; Savarino, J.; Cole-Dai, J. H.; Rai, V. K.; Thiemens, M. H. Anomalous sulfur isotope compositions of volcanic sulfate over the last millennium in Antarctic ice cores. *Journal of Geophysical Research - Atmospheres* **2008**, *113*, D20112.

(72) Bork, N.; Kurten, T.; Vehkamaki, H. Exploring the atmospheric chemistry of O2SO3- and assessing the maximum turnover number of ion-catalysed H2SO4 formation. *Atmospheric Chemistry and Physics* **2013**, *13*, 3695–3703.

(73) Mauldin, R. L.; Berndt, T.; Sipila, M.; Paasonen, P.; Petaja, T.; Kim, S.; Kurten, T.; Stratmann, F.; Kerminen, V. M.; Kulmala, M. A new atmospherically relevant oxidant of sulphur dioxide. *Nature* **2012**, *488*, 193–197.

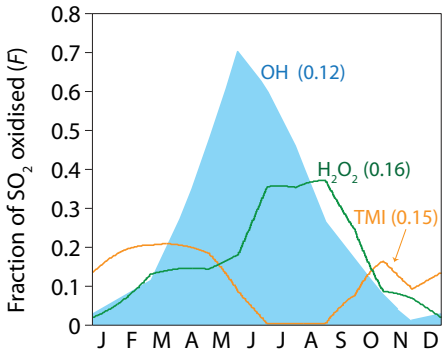

Figure 1: Fraction of SO_2 removed by oxidation by OH radicals (blue) in the gas phase, and H_2O_2 (green) and transition metal-catalysed oxidation (orange) in the aqueous phase, approximated for 45°N (*14*, *17*, *27*), considering an annual average of 43% of SO_2 is removed by oxidation (the remainder being lost through wet or dry deposition) as shown in Figure S1. The number in parentheses is the annual average SO_2 removal attributed to a particular pathway. The OH curve is filled to distinguish OH oxidation, which varies diurnally, from H_2O_2 and TMI-catalysed oxidation, which do not.

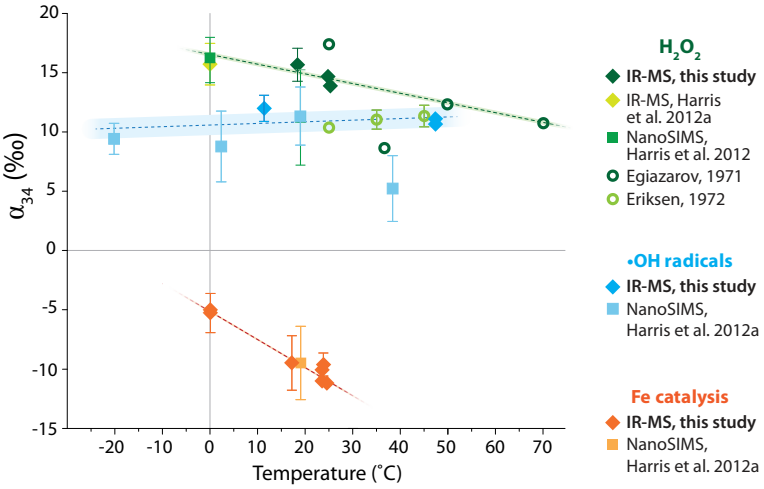

Figure 2: Temperature-dependent fractionation factors expressed in permil (i.e. $(\alpha - 1) \times 1000$) for the oxidation of SO_2 by OH radicals in the gas phase (blue), and H_2O_2 (green) and TMI catalysis (orange) in the aqueous phase. Previous measurements are also shown (*31*, *32*, *47–49*). Error bars on points show the 1σ standard deviation; error bars are not shown where the data point is larger than the 1σ error. Dotted lines show the weighted fit to the data, and the 1σ error in the fit is shown by the blocked colour area surrounding the line.

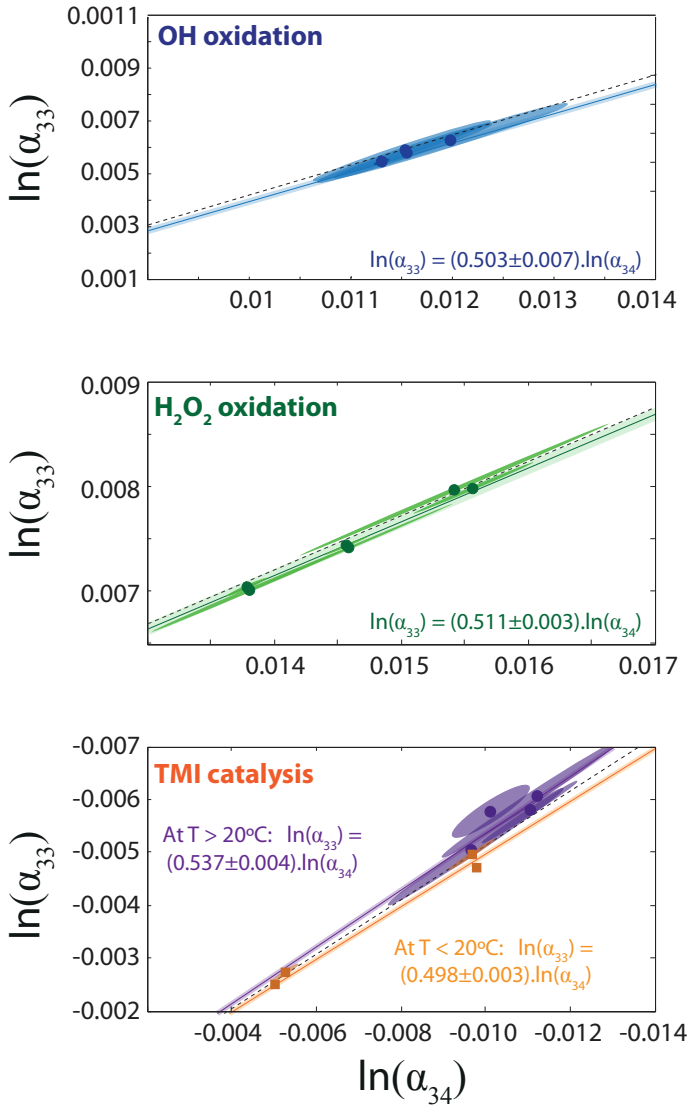

Figure 3: Relationship between α_{33} and α_{34} for the oxidation of SO_2 by a) OH radicals in the gas phase, and b) H_2O_2 and c) TMI catalysis in the aqueous phase. Ellipses show the 1σ correlated error in the data points. Solid coloured lines show the linear regression accounting for errors and correlations (*51*, *52*). The error in the regression is shown by the blocked colour area surrounding the line. The slope of the regression line represents the value of θ_{33}, and the normal 'mass-dependent' fractionation line (θ_{33} = 0.515 (*34*)) is shown as a black dashed line for comparison. For the TMI-catalysed oxidation reaction, θ_{33} is significantly different for lower- and higher-temperature experiments, and these are shown in orange (squares) and purple (circles) respectively.

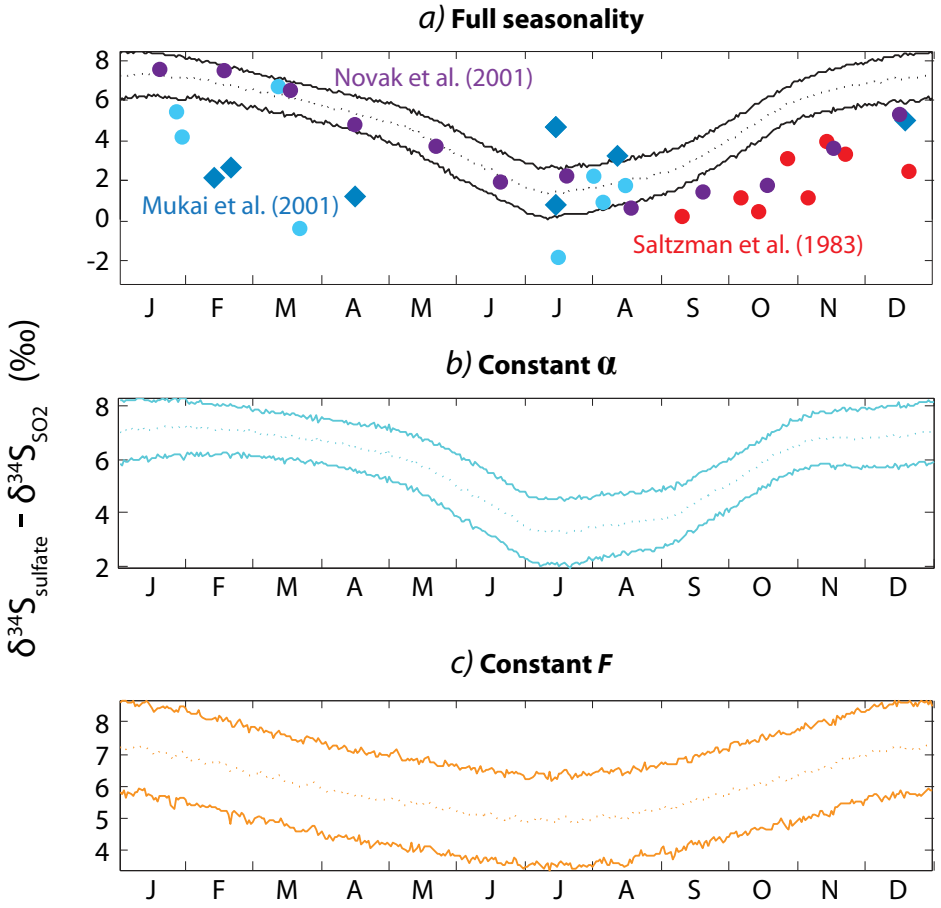

Figure 4: Modelled difference in δ^{34}S values of SO_2 and sulfate, compared to ambient observations from Novak et al. (*42*) (Czech Republic, continental, purple), Mukai et al. (*43*) (China, light blue circles = coastal, dark blue diamonds = continental) and Saltzman et al. (*44*) (North America, continental, red). The three scenarios correspond to the model runs described in Section 3.2. The dotted line shows the mean for each scenario, and the solid lines show the 1σ error in the model estimate.

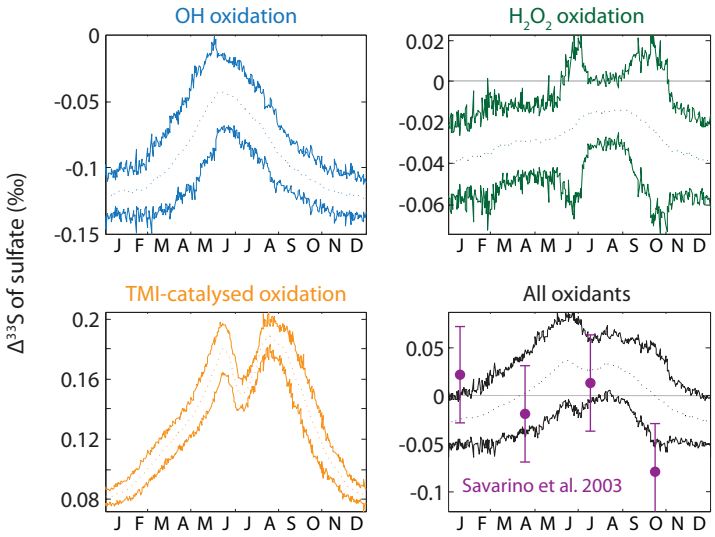

Figure 5: Model Δ^{33}S values of sulfate. The first three parts isolate changes due to a particular oxidation pathway, while the bottom right part shows the combined Δ^{33}S seasonality due to all pathways. Observations from Savarino et al. (*39*) are shown for comparison.

Oxidant	**T** (°C)	**Type**	#	f_{blank}	$f_{\text{remaining}}$	$\delta^{34}\mathbf{S}_{\text{measured}}$ (‰)	$\delta^{34}\mathbf{S}_{\text{corrected}}$ (‰)	$\alpha_{\mathbf{34}}$ (‰)
OH	11.4	Residual SO_2	1.1[a]	0.020	0.989	-0.066±0.011	-0.135±0.012	12.0±1.1
OH	47.4	Residual SO_2	1.2	0.015	0.950	-0.487±-0.014	-0.569±0.014	11.16±0.28
OH	47.4	Product H_2SO_4	1.2	0.267	0.950	8.939±0.085	10.392±0.093	10.66±0.10
OH	47.4	Residual SO_2	1.3[b]	0.019	0.950	-0.463±0.013	-0.568±0.013	11.12±0.25
H_2O_2	18.2	Product, 1^{st} bubbler	2.1	0.010	0.455	10.18±0.11	10.23±0.11	15.66±0.16
H_2O_2	18.2	Product, 2^{nd} bubbler	2.1	0.014	0.455	-2.04±0.19	-2.143±0.19	15.7±1.4
H_2O_2	25.1	Product, 1^{st} bubbler	2.2	0	0.911	13.226±0.10	13.226±0.10	13.88±0.11
H_2O_2	25.1	Product, 2^{nd} bubbler	2.2	0	0.911	11.889±0.31	11.889±0.31	13.88±0.36
H_2O_2	24.6	Product, 1^{st} bubbler	2.3	0	0.873	13.661±0.26	13.661±0.26	14.67±0.28
H_2O_2	24.6	Product, 2^{nd} bubbler	2.3	0	0.873	11.594±0.30	11.594±0.30	14.67±0.38
TMI catalysis	0	Product SO_4^{2-}	3.1	0.024	0.218	-0.816±0.25	-2.237±0.70	-5.2±1.6
TMI catalysis	0	Residual SO_2	3.1	0.241	0.218	8.259±0.073	7.662±0.068	-5.005±0.044
TMI catalysis	17.1	Product SO_4^{2-}	3.2	0.018	0.102	-1.16±0.28	-2.54±0.62	-9.7±2.3
TMI catalysis	17.1	Residual SO_2	3.2	0.293	0.102	18.57±0.19	22.45±0.23	-9.73±0.10
TMI catalysis	23.5	Product SO_4^{2-}	3.3	0	0.04	-1.504±0.027	-1.504±0.027	-11.02±0.20
TMI catalysis	23.5	Product, 2^{nd} bubbler	3.3	0	0.04	34.7±1.3	34.7±1.3	-10.08±0.10
TMI catalysis	23.8	Product SO_4^{2-}	3.4[c]	0	0.015	-0.6287±0.061	-0.6287±0.061	-9.63±0.96
TMI catalysis	24.5	Product SO_4^{2-}	3.5[c]	0	0.015	-0.73±0.33	-0.73±0.33	-11.18±0.51

[a]no Product H_2SO_4 is shown for 1.1 as the quantity produced was too small in relation to the filter blank. Reaction extent determined from SF_6 pressure in IR MS. [b]no Product H_2SO_4 as the sample jar was broken during centrifuging. Reaction extent taken to be equal to that of duplicate experiment 1.2. [c]no Product H_2SO_4 for 3.4 or 3.5 as the sample jars were broken during centrifuging. Reaction extent determined gravimetrically from washed Ag_2S.

Table 1: *previous page* - Sulfur isotope fractionation factors α_{34}) measured with IR-MS for $\delta^{34}S$ during the oxidation of SO_2 by OH radicals in the gas phase and H_2O_2 and TMI-catalysis in the aqueous phase. 'Type' shows the sample type being analysed. f_{blank} is the fraction of sulfur in the sample not representative of the reaction of interest. $f_{\text{remaining}}$ is the fraction of SO_2 remaining following oxidation. $\delta^{34}S_{\text{measured}}$ is the raw measured isotopic composition while $\delta^{34}S_{\text{corrected}}$ has been corrected for the contribution of blank sulfur; for MIT samples, no blank correction was performed as described in Section S1.5 of the supplementary material. Errors are the 1σ standard deviation as described in Section S1.6 of the supplementary material; errors were propagated through to estimate uncertainty in fractionation factors.

Table 2: Measured values of α_{34}, α_{33} and $^{33}\theta$ for the oxidation of SO_2 by the three major atmospherically relevant pathways. Errors are the 1σ standard deviation. Weighted fits represent the average $^{33}\theta$ values for each pathway, and are found from the weighted linear regression of $\ln(\alpha_{34})$ against $\ln(\alpha_{33})$. $\Delta^{33}S_{max}$ values (with θ_{33} = 0.515 (*34*)) are the maximum that could occur in product sulfate i.e. at a low reaction extent such that the SO_2 reservoir is not significantly altered.

Oxidant	**T** (°C)	α_{34} (‰)	α_{33} (‰)	$^{33}\theta$	$\Delta^{33}S_{max}$ (‰)
OH	11.4	12.0±1.1	6.06±0.95	0.505±0.090	-0.121±0.022
OH	47.4	11.16±0.28	5.6±2.0	0.50±0.17	-0.114±0.040
OH	47.4	11.12±0.25	5.7±1.1	0.515±0.097	-0.004±0.001
OH	47.4	10.66±0.10	5.32±0.50	0.500±0.047	-0.158±0.015
			Weighted fit for OH	0.503±0.007	
H_2O_2	18.2	15.66±0.16	8.00±0.31	0.513±0.020	-0.039±0.001
H_2O_2 [a]	18.2	15.7±1.4	8.0±6.3	0.515±0.403	-0.002±0.001
H_2O_2	25.1	13.88±0.11	7.07±0.14	0.511±0.011	-0.049±0.001
H_2O_2	25.1	13.88±0.36	7.03±0.16	0.509±0.017	-0.088±0.003
H_2O_2	24.6	14.67±0.28	7.47±0.09	0.511±0.012	-0.058±0.001
H_2O_2	24.6	14.67±0.38	7.44±0.17	0.509±0.018	-0.095±0.003
			Weighted fit for H_2O_2	0.511±0.003	
TMI catalysis	0	-5.2±1.6	-2.72±0.27	0.518±0.170	-0.014±0.005
TMI catalysis	0	-5.005±0.044	-2.50±0.17	0.498±0.033	0.084±0.006
TMI catalysis	17.1	-9.7±2.3	-4.95±0.25	0.511±0.127	0.036±0.009
TMI catalysis	17.1	-9.73±0.10	-4.70±0.83	0.482±0.085	0.320±0.056
			Weighted fit for TMIs, $T < 17.1°C$	0.498±0.003	
TMI catalysis	23.5	-11.02±0.20	-5.77±0.68	0.522±0.062	-0.076±0.009
TMI catalysis	23.5	-10.08±0.010	-5.74±0.85	0.568±0.087	-0.538±0.082
TMI catalysis	23.8	-9.63±0.96	-5.03±0.83	0.521±0.087	-0.057±0.009
TMI catalysis	24.5	-11.18±0.51	-6.06±0.43	0.541±0.046	-0.288±0.024
			Weighted fit for TMIs, $T > 17.1°C$	0.537±0.004	

[a]Error in α_{33} very large due to the small absolute fractionation in ^{33}S. Values of $^{33}\theta$ and $\Delta^{33}S$ are given but are not used in later analyses or included in figures.